15

Four-photon mixing in a ghost fiber endoscope

© D.A. Balakin, A.V. Belinsky¶

Moscow State University, Faculty of Physics,
119991 Moscow, Russia

¶ e-mail: belinsky@inbox.ru

Received September 19, 2023
Revised September 19, 2023
Accepted September 28, 2023

A circuit design of a fiber endoscope is described that allows monitoring of hard-to-reach cavities and other partially transparent and/or reflective objects into which it is possible to pass a thin fiber bundle.

Keywords: quantum optics, ghost images, entangled states, biphoton light sources, biophysics, medical physics.

DOI: 10.61011/EOS.2023.09.57348.5575-23

1. Introduction

The nonlinear spontaneous four-photon mixing process has good prospects for application in quantum ghost imaging. This is an emerging discipline associated with the use of spatially separated corelated light beams [1]. An object under study is irradiated by one of the beams, which is then detected by a bucket detector. The other light beam is sent to a photodetector array, and coincidences (simultaneous detections made by the collecting sensor and any photodetector) are recorded. This is not only convenient in terms of spatial selectivity, but also offers significant advantages in the context of noise cancellation and delicacy [2]. Simultaneous detection of corelated photons has long been used in imaging [3]. Ghost imaging with detection of idler photons (i.e., photons that did not interact with the examined sample) features high noise immunity due to the fact that individual background photons get rejected by a coincidence circuit [4].

It has been demonstrated recently [5–8] that, compared to three-photon spontaneous parametric down-conversion (SPDC), counter-propagating four-photon mixing provides higher-quality ghost images by improving the diffraction limit of resolution due to phase synchronism. Ghost polarimetry has also enjoyed distinct progress [9–11]. The present study is focused on potential applications of counter-propagating four-photon mixing in endoscopy.

A ghost fiber endoscope design (although without the nonlinear four-photon process) has already been proposed in [12]. The correlation of two illuminators (one for the examined object and the other for a photodetector array) was maintained via common linear scattering in a fiber in opposite directions. Femtosecond pulses were used as pump ones. Linear scattering does not provide an exact correlation between split light beams propagating toward the opposite ends of a fiber. The problem is that common linear scattering is statistical in nature, and a considerable number of photons need to be scattered so as to send roughly equal numbers in different directions and achieve exact correlation. However, this is not always acceptable from the viewpoint of gentle handling of the object under examination, which is especially important in experiments with fragile biological objects. Naturally, one may use a weaker beam to irradiate the object, but the frequency of spurious coincidences between the other beam and background noise photons increases in this case. The regime with single-photon emission and counting is the optimum one in this regard. The setup presented in Fig. 1, which is discussed below, operates in exactly this manner, since photons from pairs produced in counter-propagating four-photon mixing necessarily move toward the opposite ends of a fiber. At the same time, the single-photon emission and counting regime provides an opportunity to reduce the measurement error by filtering individual background photons.

Thus, a bundle of multimode quartz fibers is illuminated transversally by two counter-propagating pump beams produced by a single continuous-wave laser. Naturally, the illuminated section of the bundle should be exposed. Counter-propagating four-photon mixing produces pairs of photons that move toward the opposite ends of the bundle. An ideal spatial correlation of illumination at two ends of the bundle is achieved this way. A photodetector array is immediately adjacent to one end, and the other end illuminates the studied object. If it is partially transparent and we are interested in its spatial transmittance, a single detector covering the entire field (the illuminated spot) is positioned behind the object. If the reflectance distribution is of interest, another fiber (or several fibers) collecting reflected radiation should be added to the bundle of multimode quartz fibers. It has been demonstrated recently in [13] that the use of several collecting fibers and several single-pixel detectors provides an opportunity to enhance both the sensitivity and the image quality. Joint detection of reflected and transmitted radiation is also possible. The recording of coincident counts with subsequent computer processing allows one to form images of an object by applying standard ghost imaging techniques.

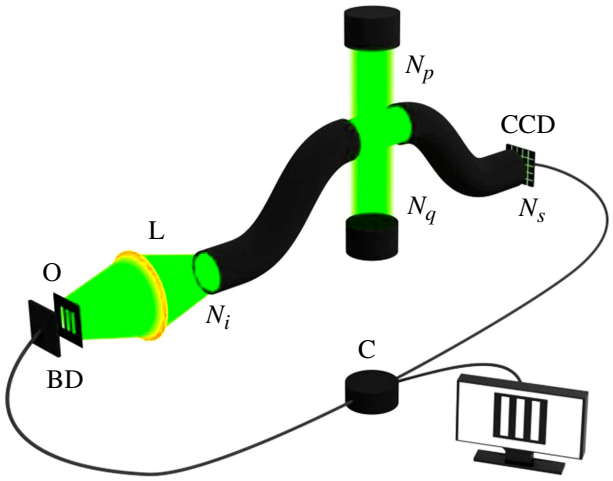

Figure 1. Setup of a fiber endoscope. Counter-propagating pump beams N_p and N_q illuminate a bundle of quartz fibers. Counter-propagating four-photon mixing produces pairs of photons N_s and N_i that move toward the opposite ends of the bundle, illuminating object O and photodetector array CCD. Intermedial projection lens L forms an image of the bundle end on the surface of the object. Light transmitted through the object is detected by bucket detector BD. The signal from correlator C is fed into a computer.

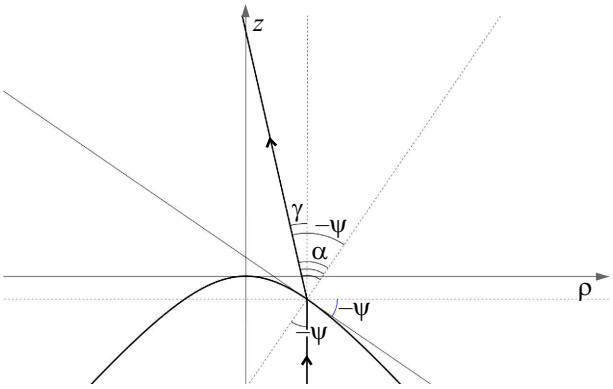

Figure 2. Diagram of focusing of a ray parallel to the optical axis by an aspherical surface with the needed angles (see text) indicated.

Ideally, the bundle end should be immediately adjacent to the object. Additional optical systems are not needed in this case. However, if contact measurements are infeasible, an intermedial projection lens needs to be inserted between the bundle and the object (see Fig. 1). The optimum case is the one of an inverting system with a linear magnification of -1. The advantages of symmetric optics, which automatically cancels out all odd aberrations, then come into play [14,15]. In the present monochromatic case, these aberrations are coma and distortion. Aspherical surfaces also allow one to get rid of spherical aberration. Thus, a single biconvex symmetric aspherical lens with parallel ray paths may be used as a projection lens in the simplest experiments of this kind. Owing to symmetry, it is sufficient to calculate just one of its surfaces: glass–air interface $s(\rho)$ that focuses an axial parallel beam to a single axial point (ρ is the distance from the optical axis).

In accordance with the Snell's law, $\sin\alpha = -n\sin\psi$ (see the notation in Fig. 2), where n is the refraction index. Since $\alpha = \gamma - \psi$, we find $\sin\psi\cos\gamma - \cos\psi\sin\gamma = n\sin\psi$. Dividing by $\cos\psi$, we obtain $\tan\psi\cos\gamma - \sin\gamma = n\mathrm{tg}\psi$. Let us express functions of angles in terms of ρ and $s(\rho)$:

$$-\mathrm{tg}\psi = s'(\rho), \tag{1}$$

$$\cos\gamma = \frac{f - s(\rho)}{\sqrt{(f - s(\rho))^2 + \rho^2}}, \tag{2}$$

$$\sin\gamma = \frac{\rho}{\sqrt{(f - s(\rho))^2 + \rho^2}}. \tag{3}$$

Here, $s(0) = 0$ and f is the vertex focal length of a symmetric half of the lens. A Cauchy problem is obtained as a result:

$$\begin{cases} \rho = (-n\sqrt{(f - s(\rho))^2 + \rho^2} + f - s(\rho))s'(\rho), \\ s(0) = 0. \end{cases} \tag{4}$$

Its solution at $n > 1$ is

$$s(\rho) = \frac{-\sqrt{(n-1)(f^2(n-1) + \rho^2(n+1))} + f(n-1)}{n^2 - 1}. \tag{5}$$

If the gap between the studied object and the bundle is filled with liquid instead of air, a glass cap in the form of a concentric meniscus with zero focal power (i.e., with roughly equal radii) needs to be installed between the lens and this liquid. Naturally, the gap between the meniscus and the lens should be filled with air. The results of above calculations remain true in this case.

Thus, a virtually ideal image limited by diffraction only is obtained at the center of the field. Since the numerical aperture of a single-mode fiber is fairly large, the influence of diffraction on the formation of an image of the bundle output end by the lens may be neglected.

As for the image field, astigmatism and field curvature, which are essentially unavoidable in single thin lenses [14,15], will still remain.

The field curvature may be compensated partially or fully by the concave fiber bundle output end. In addition, since it is by no means guaranteed that the object is flat, the image of the bundle end, which is projected onto the object, may also have a certain curvature, and imaging conditions may be optimized via longitudinal displacement of the bundle. The best option is to have concavity curvatures of equal magnitudes and different signs for the bundle and the image surface, since complete symmetry of the projection system and the corresponding advantage in odd aberrations are preserved in this case.

It is a lot more complicated when it comes to astigmatism. If one wants to compensate it, the system should not be

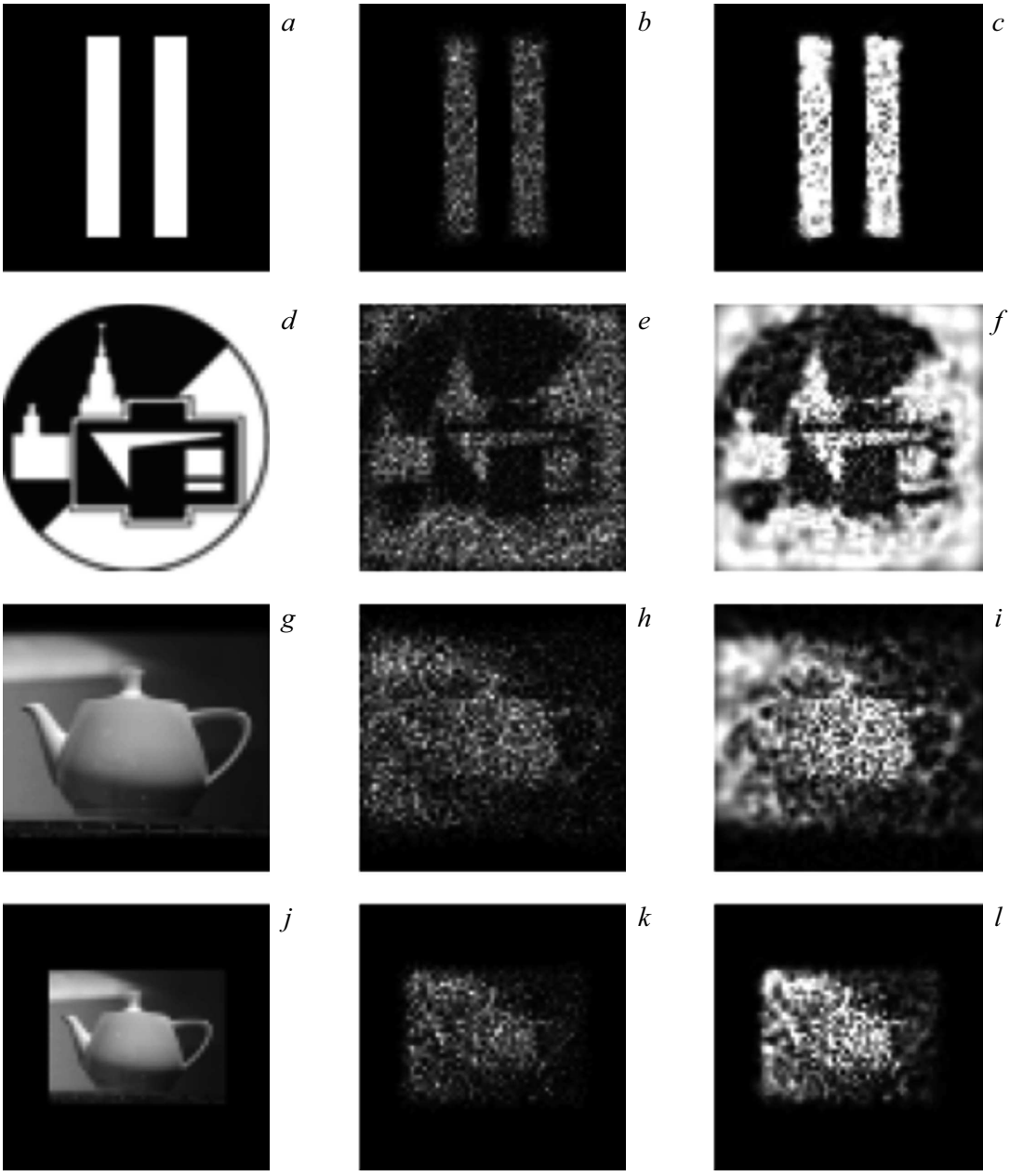

Figure 3. Results of numerical modeling of formation and processing of quantum ghost images under illumination by 10 photons/pixel on the average: left column — images of objects; middle column — obtained ghost images; right column — results of reduction of measured ghost images to the form that they would have without nonuniform blurring due to astigmatism. Quality characteristics: (*c*) PSNR = 20 dB, SSIM = 0.85, (*f*) PSNR = 16 dB, SSIM = 0.53, (*i*) PSNR = 17 dB, SSIM = 0.40, (*l*) PSNR = 20 dB, SSIM = 0.72.

thin. The simplest design of anastigmatic optics is the one with two positive lenses and an aperture diaphragm positioned between them in the symmetry plane. The system cannot be thin: an air gap comparable to the focal lengths of lenses should necessarily be left between them. If field aberrations (field curvature included) are to be compensated fully, an anastigmatic optics system becomes even longer due to the necessary addition of negative lenses. Such complications may be circumvented in the following way. If the impulse response of a single lens over the image field or its spread function with account for the field curvature and astigmatism are known, one may try to eliminate nonuniform image blurring by subsequent computer processing.

The field curvature without diffraction yields a spread function in the form of a circle (if the lens aperture is circular). Astigmatism transforms this circle into an ellipse. Both aberrations are proportional to field angle θ squared. The meridional focus of a single biconvex lens is located closer to the refraction surface than the sagittal

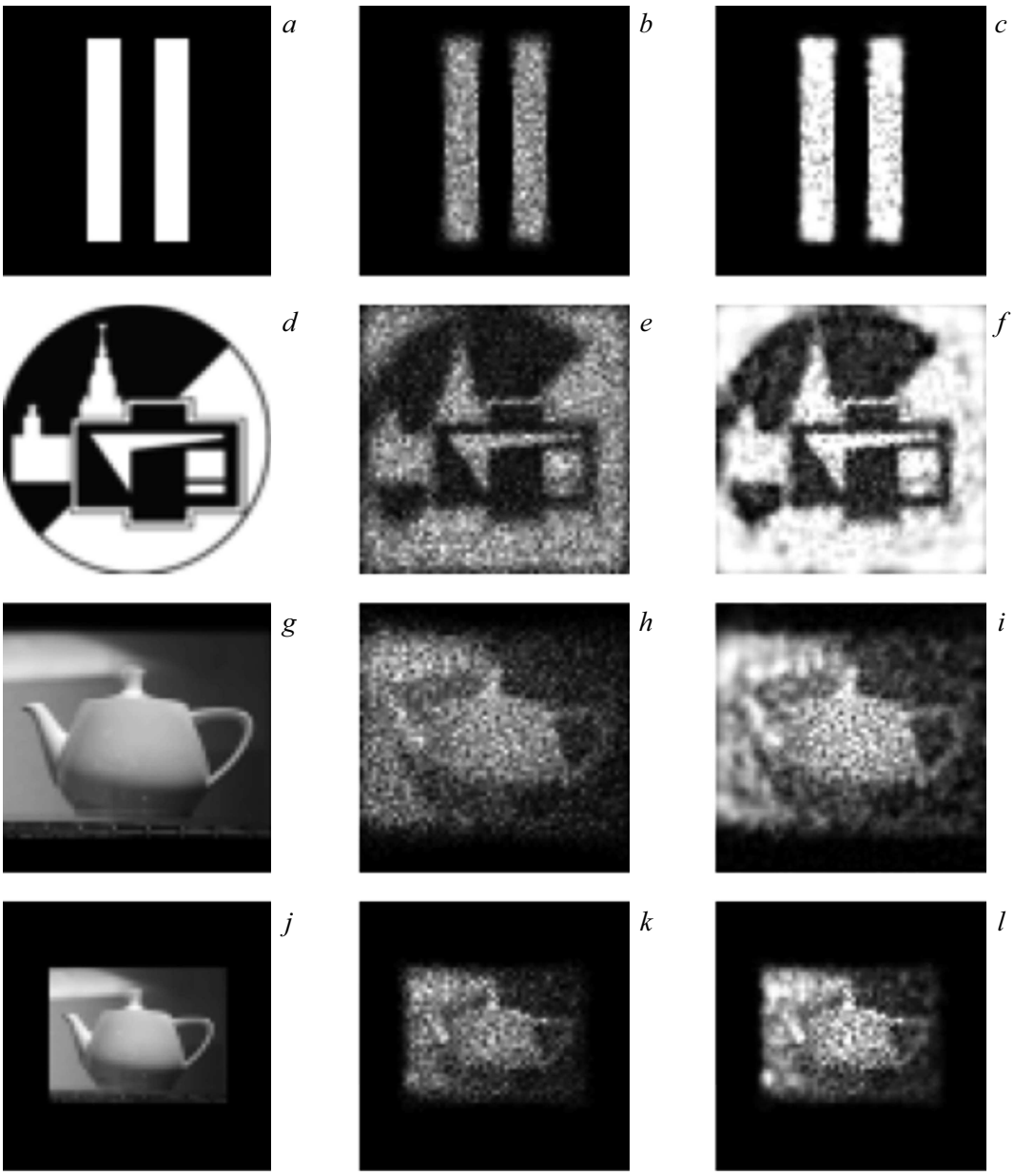

Figure 4. Results of numerical modeling of formation and processing of quantum ghost images under illumination by 30 photons/pixel on the average: left column — images of objects; middle column — obtained ghost images; right column — results of reduction of measured ghost images to the form that they would have without nonuniform blurring due to astigmatism. Quality characteristics: (*c*) PSNR = 22 dB, SSIM = 0.86, (*f*) PSNR = 18 dB, SSIM = 0.65, (*i*) PSNR = 21 dB, SSIM = 0.53, (*l*) PSNR = 23 dB, SSIM = 0.81.

one (i.e., meridional beams are focused earlier than sagittal ones [16]), and the ellipse thus gets stretched radially. This is true for a flat image surface. However, the spherical aberration on this plane is nonzero, since it is compensated fully on the surface defined by the field curvature. Thus, the design with a curved image surface located centrally between meridional and sagittal foci is the optimum one in regard to aberrations. The spread function in this case is a circle of the minimum possible size, which is specified by astigmatism. As noted above, the intensity distribution within the circle is uniform if diffraction is neglected (which is perfectly reasonable). Thus, the radius of the circle of diffusion is $r = r_0 + k\theta^2$, where r_0 is the radius of the fiber emission circle and k is a constant coefficient.

Various image processing techniques (specifically, the compressed sensing method [4,17,18] and the measurement reduction method [19]) may be used to suppress nonuniform blurring that cannot be eliminated within the traditional ghost imaging procedure. Following [4,13,20,21], we apply measurement reduction as a method that allows one to utilize the information on stochastic properties of radiation used for imaging.

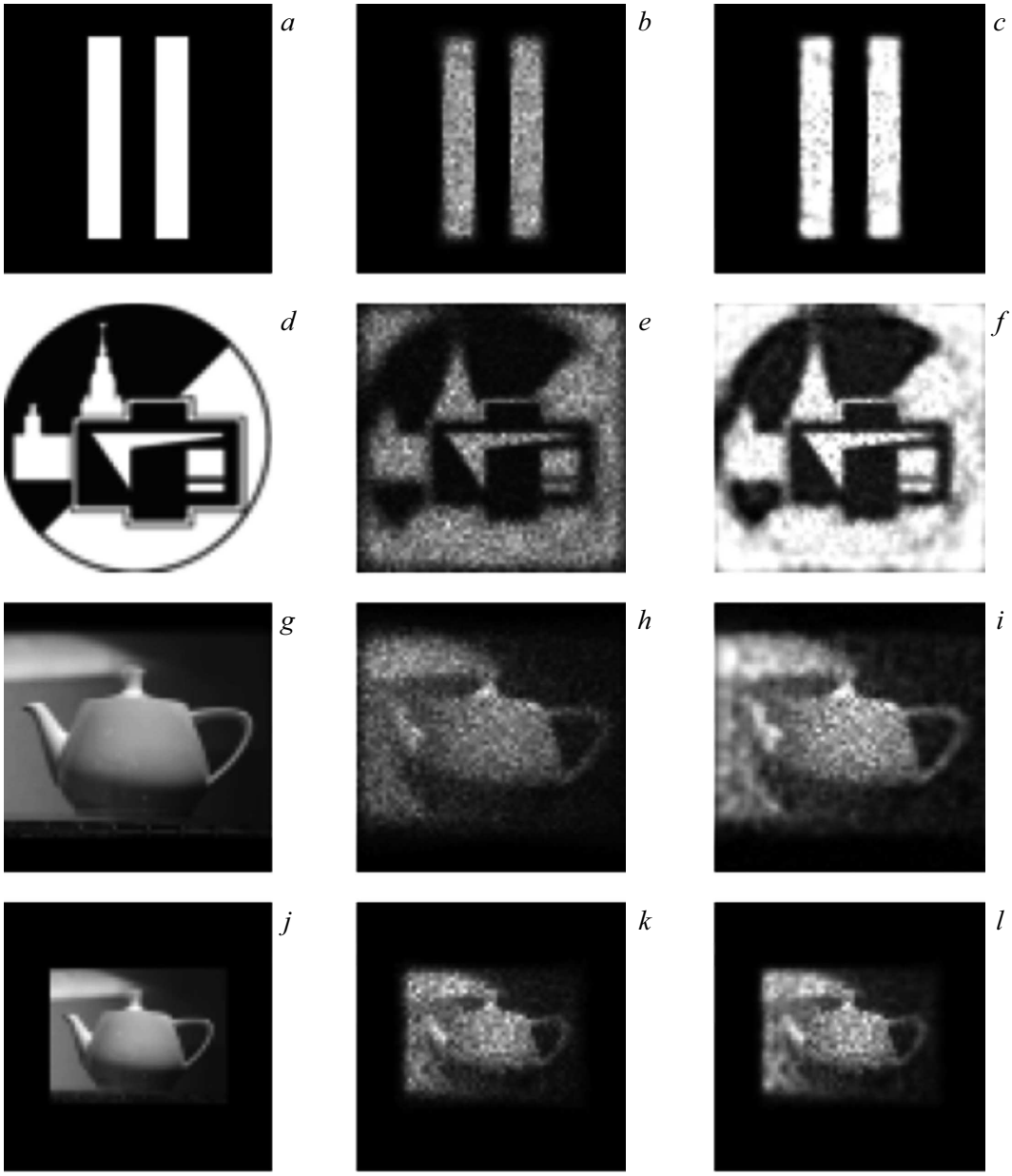

Figure 5. Results of numerical modeling of formation and processing of quantum ghost images under illumination by 100 photons/pixel on the average: left column — images of objects; middle column — obtained ghost images; right column — results of reduction of measured ghost images to the form that they would have without nonuniform blurring due to astigmatism. Quality characteristics: (*c*) PSNR = 23 dB, SSI M= 0.87, (*f*) PSNR = 20 dB, SSIM = 0.72, (*i*) PSNR = 24 dB, SSIM = 0.69, (*l*) PSNR = 27 dB, SSIM= 0.88.

In terms of the theory of computer-aided measuring systems [19], the measurement setup may be presented as $\xi = Af + \nu$, where ξ is the measured second-order correlation function as a vector with its components ξ_j $(j = 1, \ldots, K)$ being correlations between the readings of the jth photodetector (the overall number of detectors is K) and the bucket detector; f is the distribution of transmittance/reflectance of an object as an M-dimensional vector (M is the number of object pixels); operator A models the transformation of f into an average measurement result and is equal to NB^*, where N is the average number of photons illuminating each object pixel, matrix element B_{ij} of operator B represents the conditional probability that a conjugate photon interacts with the ith object pixel given that a photon is detected by the jth photodetector, and an asterisk denotes a conjugate operator; and ν is the measurement error that has zero expectation. If the number of photons emitted to each photodetector has a Poisson distribution, covariance operator Σ_ν of error ν as a stochastic vector is a diagonal one, and the variance of the jth component is $N\Sigma_{i=1}^{M} B_{ij} f_i^2$. Operator U, which models an ideal measurement instrument, is a unit one. The

following *a priori* information regarding the studied object is available:

• since transmittance/reflectance values fall within the interval from 0 to 1, f lies within the $[0,\ 1]^M$ parallelepiped;

• transmittance/reflectance values of object points located in close proximity are usually similar.

These conditions and the form of operator A dictate that the optimum procedure of measurement reduction be similar to the one considered in [20]. The following steps are repeated in it:

1. The result of linear reduction $R_*\xi = A^-\xi$ (at the first iteration) or $R_*\xi = (\Sigma^{-1/2}A)^{-1/2}$ (at subsequent iterations) is calculated using the iterative Kaczmarz method. Here, $^-$ denotes pseudoinversion, covariance operator Σ_v corresponds to the estimate of vector f obtained earlier, and estimate $\hat{f}$ of vector f formed at each internal iteration is projected onto $[0,\ 1]^M$.

2. The eigenbasis of computer-aided measuring transducer $[A, \Sigma_v, I]$ [19,21,22], which consists of eigenvectors of operator $A^*\Sigma_v^{-1}A$ in the present case, is calculated. Let us denote the operator of transition to this basis as T and the eigenvalues corresponding to eigenvectors as ϵ_i^2.

3. Vector u is formed in the following way: if $(T\hat{f})_i^2\epsilon_i^2 < \tau$, $u_i = (T\hat{f})_i$; in the contrary case, $u_i = 0$. Quantity $\tau \geq 0$ is a parameter that represents an acceptable compromise (with increasing τ) between noise suppression and the distortion of images with their components close to 0.

4. A new estimate $\hat{\hat{f}} = \Pi(T^*u)$, where Π is the projector to set $[0,\ 1]^M$, is calculated.

These steps are repeated until the change in estimate obtained after the execution of steps 1–4 becomes sufficiently small. Since the covariance error operator is diagonal in the present case, the estimate does not actually change at step 1; therefore, it is sufficient to repeat steps 2–4 only.

The results of numerical modeling of ghost imaging and reduction of images to the form free from blurring due to residual aberrations are presented in Figs. 3–5. The values of numerical quality characteristics (peak signal-to-noise ratio (PSNR) and structural similarity (SSIM) index) are indicated in the captions. It is evident that an increase in the average number of photons does little to improve the quality of the reduction result for a fairly simple object (panels (a)). This is not the case for more complex objects (especially those occupying a considerable part of the field and subjected to strong blurring; see panels (g)). It is also evident that higher-contrast images (panels (a, d)) are reconstructed better than lower-contrast ones (g, j, a). Higher-contrast features in the latter images start to reveal themselves at a lower illumination intensity.

The signal-to-noise ratio values demonstrated that the discussed method is highly resistant to shot noise and may be used with low photon fluxes, thus minimizing the risk of photodamage to samples sensitive to light (e.g., biological ones).

It is worth pointing out that ghost imaging in its fiber-optic variation has bright prospects for application. The advantages of phantom imaging can be realized in full in this case and ensure that the observations of objects under study remain unobtrusive while retaining the potential to penetrate into cavities that are difficult to examine directly.

Common techniques rely on the introduction of cameras into the human body. The sizes of these cameras are not always practical (especially in pediatrics, since the organs of a child's body are naturally smaller). Fiber bundles, which may be made as small as on the order of 1 mm in diameter, solve this problem. Such endoscopes are crucial for pediatric surgery and, in particular, neonatal surgery for preterm infants, since the organs of premature newborns and infants with congenital defects are both small in size and feature deformed morphologies and anatomic shapes [23,24].

Ultrathin endoscopes are needed not only in diagnostics, but also for real-time monitoring in surgical treatment. Such systems also hold promise for application in diagnostic and surgical endovascular procedures [25].

Funding

This study was supported by a grant from the Russian Science Foundation (project No. 21-12-00155).

Conflict of interest

The authors declare that they have no conflict of interest.

References

[1] A.V. Belinskii, D.N. Klyshko. J. Experiment. and Theor. Phys., **78** (3), 259 (1994).
[2] A. Gatti, E. Brambilla, M. Bache, L. A. Lugiato. In: *Quantum Imaging*, ed. by M.I. Kolobov (Springer, 2007), p. 79.
[3] T.B. Pittman, Y.H. Shih, D.V. Strekalov, A.V. Sergienko. Phys. Rev. A, **52** (5), R3429 (1995). DOI: 10.1103/physreva.52.r3429
[4] P.A. Morris, R.S. Aspden, J.E.C. Bell, R.W. Boyd, M.J. Padgett. Nat. Commun., **6**, 5913 (2015). DOI: 10.1038/ncomms6913
[5] A.V. Belinsky, R. Singh. J. Experimen. and Theor. Phys., **132**, 212 (2021). DOI: 10.1134/S1063776121020011.
[6] D.A. Balakin, A.V. Belinsky. Quantum Information Processing, **21** 251 (2022). DOI: 10.1007/s11128-022-03602-w
[7] D.A. Balakin, A.V. Belinsky. J. Experimen. and Theor. Phys., **133** (1), 26 (2021). DOI: 10.1134/S1063776121060091.
[8] A.V. Belinsky, V.V. Vasilkov. Opt. Spectrosc., **131**, 56 (2023). DOI: 10.21883/EOS.2023.01.55517.4060-22.
[9] S.A. Magnitskiy, D.P. Agapov, I.A. Belovolov, P.P. Gostev, D.N. Frolovtsev, A.S. Chirkin. Moscow University Physics Bulletin, **76** (6), 424 (2021). DOI: 10.3103/s0027134921060060.
[10] S. Magnitskiy, D. Agapov, A. Chirkin. Opt. Lett., **47** (4), 754 (2022). DOI: 10.1364/OL.387234
[11] D. Agapov, S. Magnitskiy, A. Chirkin. EPJ Web of Conferences, **220**, 03002 (2019). DOI: 10.1051/epjconf/201922003002
[12] A.V. Belinsky, P.P. Gostev, S.A. Magnitskiy, A.S. Chirkin. JETP Lett., **117**, 202 (2023). DOI: 10.1134/S0021364022602718

[13] D.A. Balakin, A.V. Belinsky. J. Experimen. and Theor. Phys., **137** (6), 785 (2023). DOI: 10.1134/S1063776123120038
[14] G.G. Slyusarev. *Metody rascheta opticheskikh sistem* (Mashinostroenie, L., 1969) (in Russian).
[15] G.G. Slyusarev. *Raschet opticheskikh sistem* (Mashinostroenie, L., 1975) (in Russian).
[16] B.G. Begunov. *Geometricheskaya optika* (Izd. Mosk. Gos. Univ., M., 1966) (in Russian).
[17] G.M. Gibson, S.D. Johnson, M.J. Padgett. Opt. Express, **28** (19), 28190 (2020). DOI: 10.1364/oe.403195
[18] E.J. Candes, T. Tao. IEEE Trans. Inf. Theory, **52** (12), 5406 (2006). DOI: 10.1109/tit.2006.885507
[19] Yu.P. Pyt'ev. *Metody matematicheskogo modelirovaniya izmeritel'no-vychislitel'nykh sistem*, 3rd ed. (Fizmatlit, M., 2012) (in Russian).
[20] D.A. Balakin, A.V. Belinsky. Quantum Electronics, **49** (10), 967 (2019).
[21] D.A. Balakin, D.P. Agapov, P.P. Gostev, S.A. Magnitskiy, D.N. Frolovtsev, A.S. Chirkin. JETP, **135** (6), 779 (2022). DOI: 10.1134/S1063776122120159.
[22] D.A. Balakin, Yu.P. Pyt'ev. Pattern Recognition and Image Analysis, **31** (4), 601 (2021). DOI: 10.1134/S1054661821040040
[23] G.I. Lukomskii, Yu.E. Berezov. *Endoskopicheskaya tekhnika v khirurgii* (Meditsina, M., 1967) (in Russian).
[24] S.Ya. Doletskii, V.P. Strekalovskii, E.V. Klimanskaya, O.A. Surikova. *Endoskopiya organov pishchevaritel'nogo trakta u detei* (Meditsina, M., 1984) (in Russian).
[25] I.V. Fedorov, B.I. Sigal, V.V. Odintsov. *Endoskopicheskaya khirurgiya* (Meditsina, M., 2001) (in Russian).

Translated by D.Safin